ChemPubSoc Europe
DOI: 10.1002/cphc.201800965
CHEMPHYSCHEM Articles

Tuning the Magnetic Properties of Columnar Benzo[*e*][1,2,4]triazin-4-yls with the Molecular Shape

Marcin Jasiński,[a] Katarzyna Szymańska,[a] Anita Gardias,[b] Damian Pociecha,[c] Hirosato Monobe,[d] Jacek Szczytko,[b] and Piotr Kaszyński[a, e, f]

Dedicated to Professor Janusz Zakrzewski of University of Łódź on the occasion of his 70th birthday.

A homologous series of disc-like 1,3,6-trisubstituted benzo[*e*][1,2,4]triazin-4-yls **1[n]** was synthesized and their structural, thermal, optical, magnetic, and electric properties were investigated. The results demonstrate that all members of the series display a Col_h phase with clearing temperatures depending on the length of the alkoxy chains at the N(1) position, hence the shape of the disc. Powder XRD and magnetic data indicate a gradual change in the column diameter and magnetic behavior in the series in transition from half-disc in **1[0]** (antiferromagnetic interactions) to full-disc geometry in the **1[12]** homologue (ferromagnetic interactions with $J/k_B = +7.5$ K). Studies of binary systems revealed that a 1:1 mixture of **1[0]** and **1[12]** exhibits modest stabilization of the Col_h phase with an expanded range, and magnetic behavior typical for **1[0]** in the rigid phase obtained from the melt. Electric measurements demonstrated hole mobility of $\sim 10^{-3}$ cm^2 V^{-1} s^{-1} and dark conductivity of $\sim 10^{-11}$ Scm^{-1} in the mixture and individual compounds. The latter is enhanced up to 4 times by simultaneous illumination with UV light.

1. Introduction

There is an increasing interest in organic spin-containing molecules as potential materials for information processing and bottom up fabrication of organic spintronic devices,[1] such as spin valves and spin filters.[2] The advantage of organic compounds over inorganic materials lies in weak spin-orbit coupling and hyperfine interactions,[1b] and consequently relatively long spin lifetime and spin diffusion lengths.[3] One approach to such devices involves a hierarchical self-assembly of nano-sized structures, e.g. paramagnetic microtubes and vesicles,[4] that exhibit charge and spin transport properties. Another attractive way to organize organic paramagnetic materials is to use self-assembly properties of liquid crystals.[5] For instance, disc-like molecules self-organize in unidimensional channels and many columnar discotic phases exhibit semiconductive properties and high charge mobility.[6] The highest mobility is observed in aligned columnar liquid crystalline phases with either homeotropic (face-on) orientation of columns (attractive for e.g. photovoltaic cells) or planar (edge-on) orientation desired in field-effect transistors.

Recently, we reported[7] discotic materials derived from the exceptionally stable benzo[*e*][1,2,4]triazin-4-yl[8] in which the electron spin is delocalized in the π-system of the rigid core. Preliminary experiments indicated that the contact of the π faces and hence the type of spin-spin interactions is controlled by the peripheral substituents. Thus, compound **1[0]** with a small substituent at the N(1) position (Figure 1) exhibits strong antiferromagnetic interactions, while **1[12]** derivative shows weak ferromagnetic spin-spin exchange interactions. In addition, both derivatives exhibit photoinduced charge carrier (hole) mobility (μ_h) of about 1.4×10^{-3} cm^{2}V^{-1}s^{-1} in partially aligned samples. For further development of this type of molecular materials for molecular electronics and spintronic applications it is important to understand the origin of the observed structure-dependent magnetic behavior through systematic investigation of the homologous series.

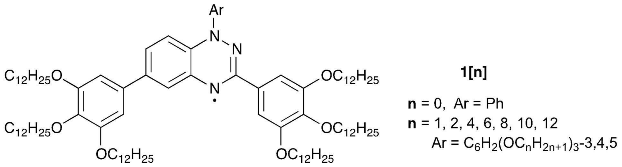

Figure 1. The structure of members of homologous series **1[n]**.

---

[a] Dr. M. Jasiński, K. Szymańska, Prof. P. Kaszyński
Faculty of Chemistry, University of Łódź
Tamka 12, 91-403 Łódź, Poland
[b] A. Gardias, Dr. J. Szczytko
Institute of Experimental Physics, Faculty of Physics University of Warsaw, Pasteura 5, 02-093 Warsaw, Poland
[c] Dr. D. Pociecha
Faculty of Chemistry, University of Warsaw, Żwirki i Wigury 101, 02-089 Warsaw, Poland
[d] Dr. H. Monobe
National Institute of Advanced Industrial Science and Technology (AIST), Kansai Centre, Ikeda, Osaka 563-8577, Japan
[e] Prof. P. Kaszyński
Centre of Molecular and Macromolecular Studies
Polish Academy of Sciences
Sienkiewicza 112, 90-363 Łódź, Poland
E-mail: piotrk@cbmm.lodz.pl
[f] Prof. P. Kaszyński
Department of Chemistry, Middle Tennessee State University, Murfreesboro, TN 37132, USA

Supporting information for this article is available on the WWW under https://doi.org/10.1002/cphc.201800965.

Herein, we report the behavior of a homologous series **1[n]** containing even members of the series. We report thermal, magnetic and electric behavior in the series and for binary mixtures of two terminal homologues.

2. Results

2.1. Synthesis

Radicals in series **1[n]** were obtained in typical yields of 70–90% using our recently reported protocol[7,9] involving addition of ArLi to benzo[*e*][1,2,4]triazine **2** followed by aerial oxidation of the intermediate anion (Scheme 1). The ArLi reagents were generated from the corresponding ArBr **3[n]** and *t*-BuLi. The benzo[*e*][1,2,4]triazine **2** was prepared as shown in Scheme 1.

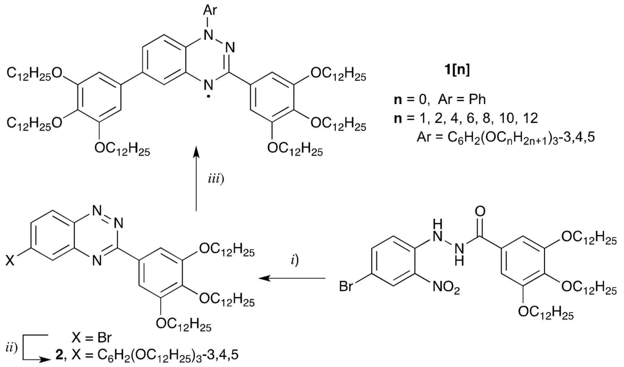

Scheme 1. Synthesis of benzo[*e*][1,2,4]triazinyl derivatives **1[n]**. *Reagents and conditions*: *i)* 1) Sn, AcOH, rt 2 hrs, reflux 25 min 2) $NaIO_4$, $MeOH/CH_2Cl_2$; *ii)* 3,4,5-$(C_{12}H_{25}O)_3C_6H_2B(OH)_2$, $Pd(PPh_3)_4$, K_2CO_3, THF/H_2O, reflux 24 hr; *iii)* 1) ArLi, THF, 2) air.

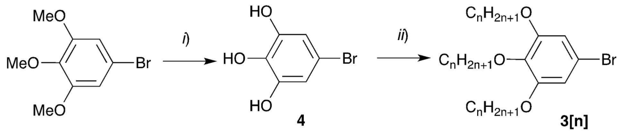

Scheme 2. Synthesis of 3,4,5-trialkoxybromobenzenes (**3[n]**). *Reagents and conditions*: *i)* BBr_3, CH_2Cl_2, −78 °C to rt, 16 h; *ii)* alkyl bromide (3.3–4.0 equiv.), K_2CO_3, DMF, 80 °C, 24 hrs.

The requisite 3,4,5-trialkoxybromobenzenes (**3[n]**) were obtained by alkylation of 3,4,5-trihydroxybromobenzene (**4**, Scheme 2)[10] according to a general literature procedure.[11]

2.2. Thermal and Optical Characterization

Thermal behavior of compounds in series **1[n]** was investigated by differential scanning calorimetry (DSC) and polarized optical microscopy (POM). The results are shown in Table 1 and Figures 2–4.

Analysis of data in Table 1 demonstrates that all compounds exhibit a columnar hexagonal phase (Col_h) with characteristic textures as shown for **1[8]** in Figure 2. Upon substitution of the N(1)–Ph ring in **1[0]** with three OMe groups, the mesophase is stabilized by 20 K. Extension of the alkyl chain leads to a decrease of the mesophase stability, which for **1[4]** and **1[6]** homologues is monotropic (Table 1, and Figure 3) with the lowest in the series Col_h–I transition temperatures. Further increase of the chain length gradually brings the clearing temperature up to above 70 °C. The variation of transition temperatures in the homologous series is shown graphically in Figure 4.

Table 1. Transition temperatures [°C] and enthalpies (kJ mol^{-1}, in italics) for **1[n]**.[a]

n	Ar	Phase behavior
0	Ph[b]	Cr 46 (*49.2*) *Col*$_h$ 73 (*6.0*) I
1	C_6H_2-3,4,5-$(OCH_3)_3$	Cr 64 (*86.9*) *Col*$_h$ 93 (*5.9*) I
2	C_6H_2-3,4,5-$(OC_2H_5)_3$	Cr 69 (*72.9*) *Col*$_h$ 76 (*4.9*) I
4	C_6H_2-3,4,5-$(OC_4H_9)_3$	Cr 60 (*72.1*) [*Col*$_h$ 50 (*6.6*)][c] I
6	C_6H_2-3,4,5-$(OC_6H_{13})_3$	Cr 61 (*69.4*) [*Col*$_h$ 52 (*6.8*)][c] I
8	C_6H_2-3,4,5-$(OC_8H_{17})_3$	Cr 57 (*51.9*) *Col*$_h$ 64 (*11.0*) I
10	C_6H_2-3,4,5-$(OC_{10}H_{21})_3$	Cr 64 (*83.5*) *Col*$_h$ 72 (*13.9*) I
12	C_6H_2-3,4,5-$(OC_{12}H_{25})_3$[b]	Cr 67 (*85.7*) *Col*$_h$ 75 (*15.2*) I

[a] Peak temperatures obtained on first heating: Cr = crystal, *Col*$_h$ = columnar hexagonal, I = isotropic; enthalpy of transition in parentheses. [b] Ref. [7] [c] Monotropic transition temperature obtained on heating.

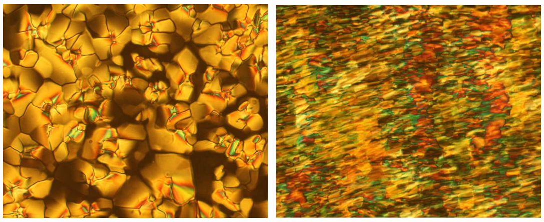

Figure 2. Left: optical texture of a *Col*$_h$ phase obtained for **1[8]** upon cooling from the isotropic phase. Right: the same phase after sheering.

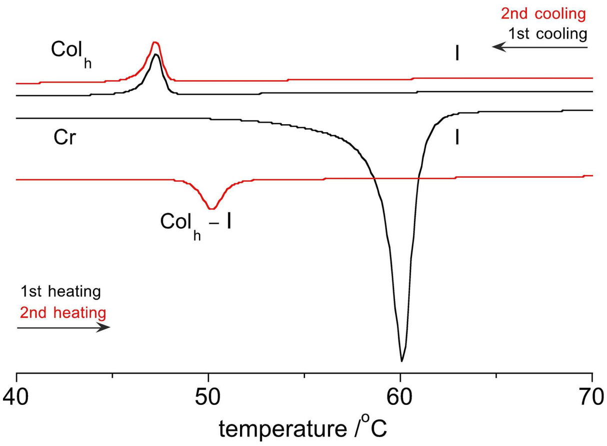

Figure 3. DSC trace of **1[4]**. The heating and cooling rates are 5 K min^{-1}.

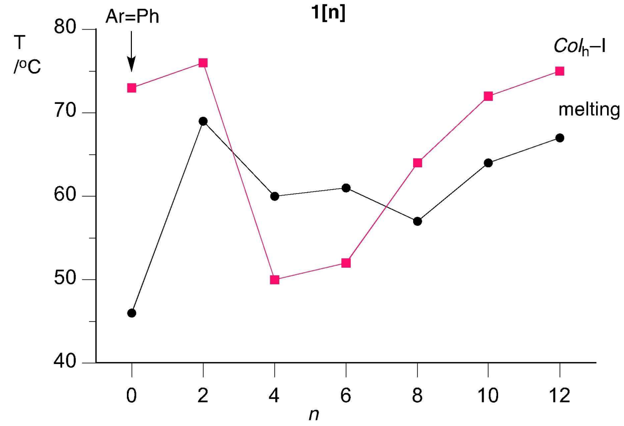

Figure 4. Phase diagram for homologous series **1[n]**.

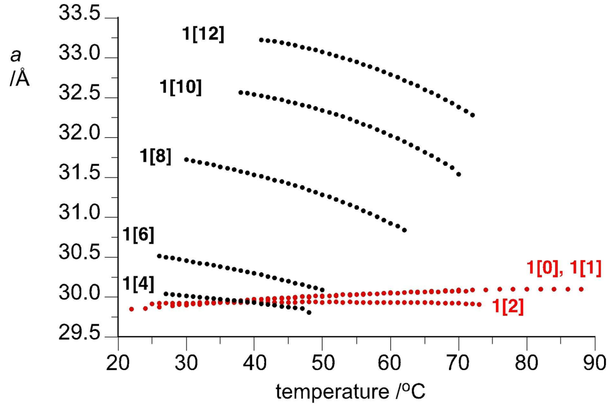

Figure 6. Temperature dependence of the lattice parameter *a* in the homologous series **1[n]**.

2.3. Phase Structure

X-ray diffraction (XRD) method was used to confirm the phase identification made on the basis of optical textures. All homologues **1[n]** gave qualitatively the same diffraction patterns, with a series of sharp, Bragg-type reflections at low angle and two broad signals at high angle range (Figure 5). Low angle peaks, which positions in *q*-space are in a ratio $1{:}\sqrt{3}{:}2$, point to a long-range positional order of columns that are arranged in a two-dimensional hexagonal lattice, with a lattice parameter *a* (column diameter) corresponding roughly to the dimension of a single molecule. Interestingly, the lattice parameter *a* exhibits different dependence on temperature for short- and long-tail homologues: the thermal expansion coefficient is positive for **1[0]**, **1[1]** and **1[2]**, while it is negative for **1[4]** and higher homologues (Figure 6). This cross-over is also visible in a comparison of lattice parameter values *a* for all homologues **1[n]**, measured at 10 K below the *Col*$_h$–I transition (Figure 7). Thus, for $n \leq 4$ the column diameter is essentially independent on the length of terminal chains attached to N(1)–Ph ring, while it linearly increases for longer homologues.

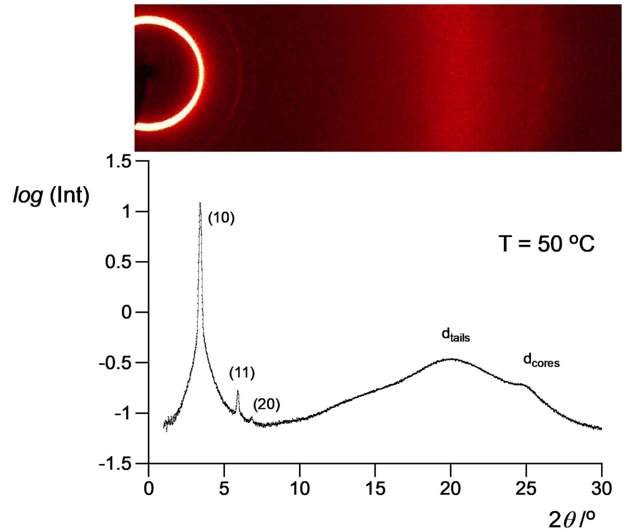

Figure 5. X-ray diffractogram for **1[2]** obtained by integration of the 2D pattern at 50 °C (inset): *Col*$_h$, $a = 29.8$ Å, diffused 4.4 Å and 3.6 Å.

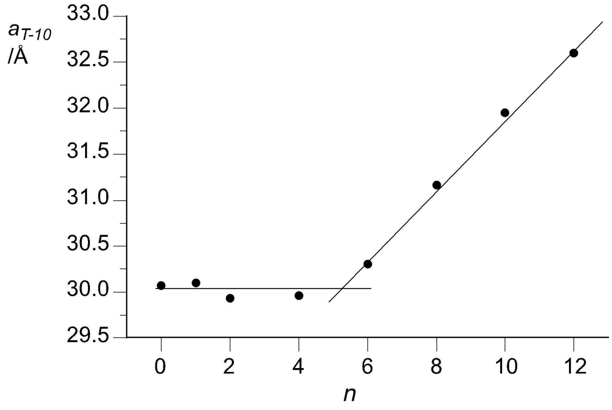

Figure 7. Lattice parameter *a* in the homologous series **1[n]** obtained at $T_{Colh} - 10$ K.

Two broad diffraction signals detected in the high angle range (Figure 5) indicate short-range (liquid-like) positional correlations of molecules along the columns, which are characteristic of disordered-type LC columnar phases. Their positions reflect the mean distance between aliphatic chains and the mesogenic cores, and they are practically temperature independent for each compound. It should be noted that the former signal is essentially independent on the homologue and is typically 4.4–4.5 Å, while the latter slightly increases with increasing *n*, from 3.4 Å for **1[0]** to 3.7 Å for **1[12]**. The growing separation between the discs along the columns is presumably due to the increasing steric demands of the elongated alkoxy chains. Analysis of the shape of this signal in **1[2]** (Figure 5) indicates a slight increase of the correlation length of positional order of molecules along the column from 15 Å to 17 Å upon cooling from 80 °C to 30 °C.

2.4. Magnetic Characterization

Magnetic susceptibility measurements in series **1[n]** revealed significant and diverse intermolecular spin-spin interactions, which are dependent on the alkyl chain length and thermal history of the sample.

Analysis of pristine crystalline samples of **1[n]** demonstrated weak ferromagnetic interactions in the solid state for homologues $n \geq 6$. This is evident from the upturn of the $\chi_p \cdot T(T)$ curve, as shown for **1[6]** in Figure 8. Assuming close π-stacked arrangements of molecules in the solid phase (similar to those in the Col_h) and hence 1-D Heisenberg ferromagnetic chain model, the magnitude of these interactions was estimated with Baker's high temperature series expansion[12] (eq 1) at $J/k_B = 2.20(1)$ K.

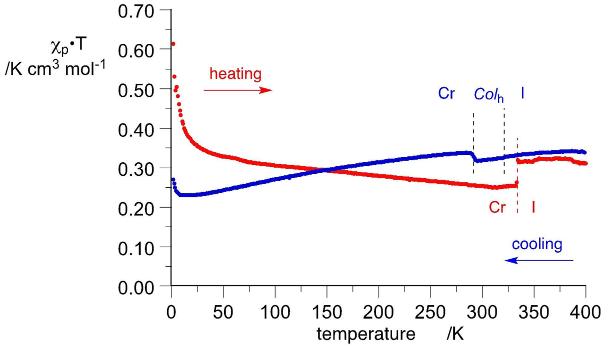

Figure 8. $\chi_p \cdot T$ *versus* temperature plot for **1[6]** obtained on heating of a pristine sample (red) and subsequent cooling (blue). Temperature change rate 0.8 K min^{-1}, field 0.1 T.

$$\chi_p = \frac{N_A g^2 \mu_B^2}{4 k_B T} \times A \tag{1}$$

in which

$$A = \left[\frac{1 + 5.797991x + 16.902653x^2 + 29.376885x^3 + 29.832959x^4 + 14.036918x^5}{1 + 2.7979916x + 7.008678x^2 + 8.6538644x^3 + 4.5743114x^4} \right]^{\frac{2}{3}}$$

and

$$x = \frac{J}{2 k_B T}$$

Upon heating above 300 K homologues melt and form fluid phases. As shown for **1[6]** in Figure 8, the abrupt increasing of the paramagnetic character of the sample at 334 K coincides with melting to an isotropic liquid. The resulting paramagnetic liquid moves in the capsule, which results in changing geometry and difficulties in centering of the magnetic signal. In addition, all homologues **1[n]** exhibit significant diamagnetic anisotropy, which makes isotropic and general Pascal constants unreliable to calculate the diamagnetic contribution. Therefore, the diamagnetic correction χ_{dia}, which accounts for the sample and the sample holder, was established by assuming paramagnetic saturation in the isotropic phase, which implies the horizontal $\chi_p \cdot T(T)$ plot. This analysis was performed separately for data obtained in heating and cooling cycles for each homologue. Details are provided in the ESI.

Cooling of **1[6]** from the isotropic phase results in a steady increase of the antiferromagnetic interactions with a slight decrease of magnetization at the I→Col_h transition (Figure 8). Upon crystallization at 292 K the number of free spins increases by 8%. Finally, below 10 K the $\chi_p \cdot T$ curve shows an upturn indicative of ferromagnetic interactions. Similar analysis was performed for other members of the homologous series and their $\chi_p \cdot T(T)$ plots for the cooling cycle are shown in Figure 9.

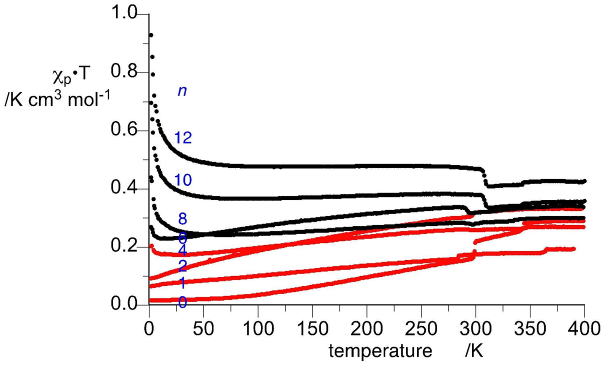

Figure 9. $\chi_p \cdot T$ *versus* temperature plots for **1[n]** obtained on cooling (0.8 K min^{-1}) at 0.1 T. Red: lower members ($n = 0$–4); black: higher members ($n = 6$–12).

Analysis of results for the homologous series demonstrates that antiferromagnetic interactions are becoming weaker with increasing length of the alkyl chain (increasing n). This is evident from the increasing paramagnetic character of the isotropic liquid, for which the $\chi_p \cdot T$ value changes from about 0.19 K cm^3 mol^{-1} for **1[1]** to 0.43 K cm^3 mol^{-1} for **1[12]** (Figure 9). A similar change is observed for the Col_h→Cr transition. While magnetization slightly decreases upon crystallization for **1[0]**, **1[1]** and **1[4]**, it clearly increases starting with homologue **1[6]** up to 13% for **1[12]**. On the other hand, at the I→Col_h transition the magnetic moment slightly decreases for all members of the series with the largest decrease for **1[0]** (12%) and smallest for **1[4]** and **1[6]**. Thus, organization of molecules in columns results in small increase of antiferromagnetic interactions, while crystallization of the columnar phase results in an onset of ferromagnetic interaction for higher homologues. An estimate of the magnitude of these ferromagnetic interactions with Baker's function (eq 1) demonstrates again increasing ferromagnetic character of the intermolecular interactions in the

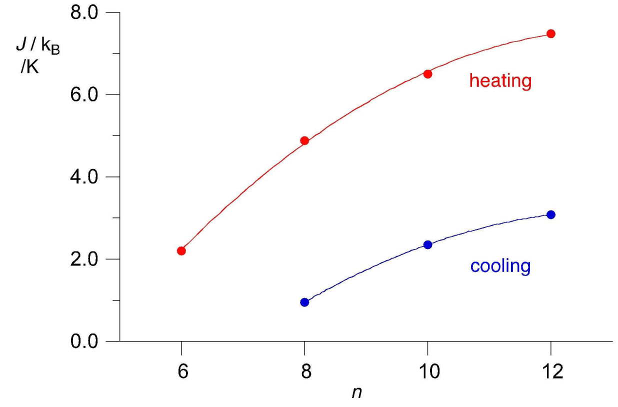

Figure 10. Exchange interaction values J/k_B obtained for **1[n]** on heating of pristine samples (red) and on cooling from the isotropic liquid (blue) at a rate 0.8 K min^{-1} at 0.1 T.

crystalline phase of series **1[n]** (Figure 10). Analysis of the results shows that stronger exchange interactions are observed in pristine crystalline samples than in solid samples obtained by crystallization of the liquid. This difference might be due to partial glassification of the columnar phase and incomplete crystallization, previously observed for **1[12]**.[7]

Further analysis of **1[12]**, with a full disc molecular shape and the largest in the series ferromagnetic exchange interactions (Figure 10), was performed at a constant temperature and variable magnetic field, B. Thus, magnetization data, $M_p(B)$, for **1[12]** obtained at 2 K confirmed the variable temperature measurements and demonstrated good fit to the Bruillouin function for $S=5/2$ or 3 (Figure 11).

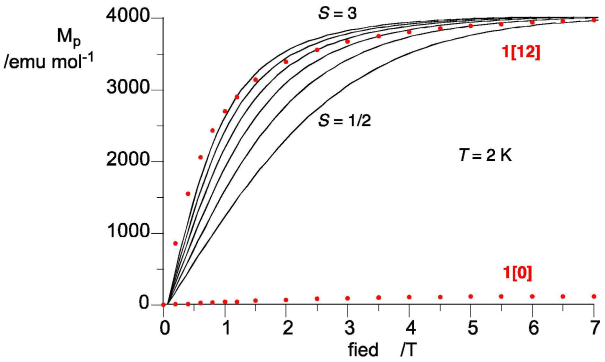

Figure 11. Paramagnetic component of molar magnetization (M_p) as a function of applied field measured for **1[0]** and **1[12]** at 2 K. The solid lines represent Brillouin functions for spin state $S=1/2$, $S=1$, $S=3/2$, $S=2$, $S=5/2$ and $S=3$.

The observed intermolecular spin-spin interactions in **1[n]** are significantly stronger than those found in mesogenic derivatives of 6-oxoverdazyl,[13] triphenylmethyl,[14] nitroxyl,[15] and bent-core benzo[*e*][1,2,4]triazinyl,[16] in which spins are largely isolated. The diverse nature of these spin-spin interactions is presumably due to different overlap of the spin-containing central heterocyclic rings governed by steric requirements of the molecules undergoing nanosegregation of the rigid and flexible parts (column formation) during the phase transition. Thus, nanosegregation results in co-facial π–π interactions most likely with antiparallel molecular orientation, as shown for **4** in Figure 12, an all-methoxy analogue of **1[1]**. The length of the alkyl chains of the N(1)–Ar substituent affects the relative position of the π systems, hence the overlap of positive and negative spin densities (Figure 12) and resulting from it magnetic interactions, according to the McConnell's model.[17] Thus, for homologues **1[0]**, **1[1]**, **1[2]** and **1[4]** with short alkyl chains, column self-assembly allows for relatively little restricted π–π contacts with favourable aniferromagnetic spin-spin interactions, as evident from essentially constant column size of about 30 Å (Figure 7). For molecules with longer alkyl substituents, nanosegregation of aliphatic and aromatic segments apparently overrides the preference for low spin system. To accommodate the increasing steric demand of the longer alkyl chains, the relative positions of the π faces are shifted, which changes the type of overlap between the heterocycles and gives rise to weak ferromagnetic exchange interactions. The effect of this steric demand on column geometry is evident from increasing column size (Figure 7) and inter-core separation.

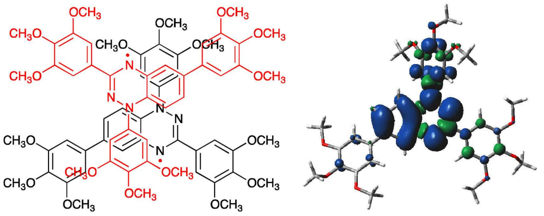

Figure 12. Nona-methoxy derivative **4**. Left: antiparallel alignment of two molecules. Right: total spin density map.

2.5. Binary Mixtures

Binary mixtures of two extreme members of the homologous series, **1[0]** and **1[12]**, exhibiting the most diverse magnetic and steric properties were prepared in ratios 1:3, 1:1 and 3:1 and the partial phase diagram is shown in Figure 13.

The graph in Figure 13 shows that despite mixing of molecules with two different shapes, the Col_h–I transition is not depressed, as it might be expected. On the contrary, the 1:1 mixture exhibits a small stabilization of the Col_h relative to the pure components. Interestingly, the 1:1 mixture could be considered as a mimic of homologue **1[6]**, for which the Col_h–I transition at 52 °C (Table 1) is 27 K lower than for the **1[0]**–**1[12]** mixture.

While the Col_h–I transition is little affected by the composition of the mixture and remains at about 75 °C, melting is suppressed by over 25 K and two mixtures, 1:3 and 1:1, melt below 20 °C (Figure 13). This greatly expands the range of the columnar phase, which is attractive in the context of applica-

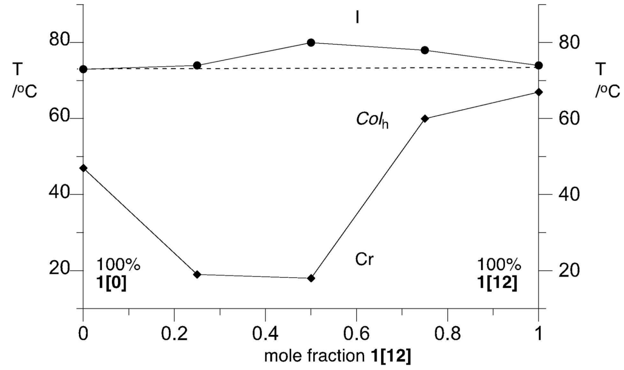

Figure 13. Partial phase diagram for a binary system of **1[0]** and **1[12]** Cr–*Col*$_h$ transition: diamonds, *Col*$_h$–I transition: full circles. The dashed line connects the *Col*$_h$–I transition for pure components.

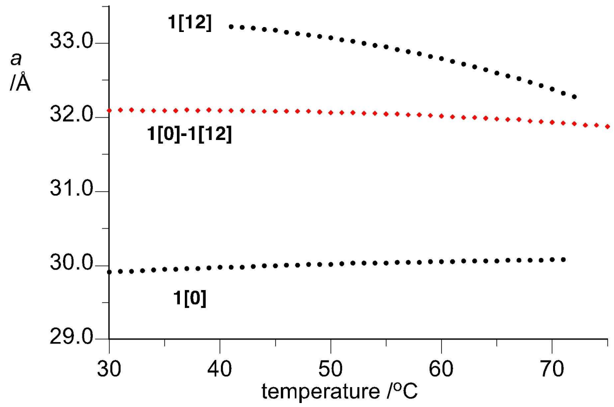

Figure 14. Temperature dependence of the lattice parameter *a* in pure derivatives **1[0]** and **1[12]** (black dots) and their 1:1 binary mixture (red diamonds).

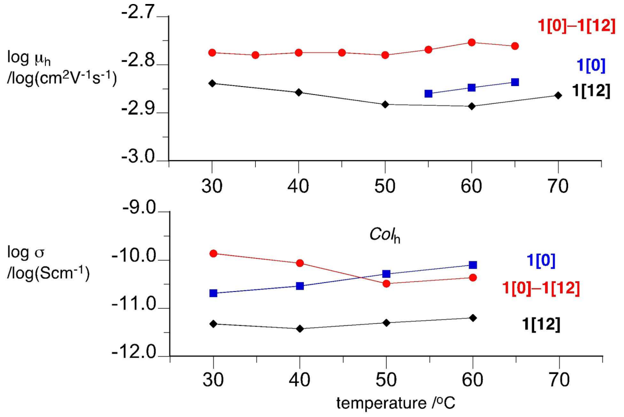

Figure 15. Top: temperature dependence of positive carrier mobility μ_h obtained by the TOF method for **1[0]**, **1[12]** and 1:1 binary mixture **1[0]**–**1[12]** at 337 nm. Electric field strength 50 or 60 kV cm^{-1}. Bottom: dark conductivity for **1[0]**, **1[12]** and 1:1 binary mixture **1[0]**–**1[12]**.

tions. For this reason, the phase structure, magnetic and conducive properties of the 1:1 binary mixture **1[0]**–**1[12]** were briefly investigated.

Powder XRD analysis of the 1:1 mixture **1[0]**–**1[12]** confirmed the formation of a columnar hexagonal phase, *Col*$_h$, and revealed that the value of the lattice parameter *a* is close to that of pure **1[12]**, while its very weak temperature dependence is reminiscent of that of **1[0]** (Figure 14). One possible interpretation of this result is that the two homologues form mixed stacks and that the less voluminous N(1)–Ph group in **1[0]** derivative provides the necessary space for the more sterically demanding dodecyloxy chains of the N(1) substituent in **1[12]**. Consequently, the alkoxy chains undergo little conformational change and the column diameter remains approximately constant in the temperature range.

TOF transient photocurrent measurements revealed that the positive charge mobility, μ_h, in an unaligned multidomain sample of 1:1 mixture **1[0]**–**1[12]** is slightly higher than that in the pure components[7] and about 1.7×10^{-3} cm^{2}V^{-1}s^{-1} in the entire range 30–70 °C (Figure 15). It should be noted, that while for pure **1[12]** the *Col*$_h$ phase is metastable at 30 °C, in the mixture thermodynamic stability of the mesophase extends to 20 °C. The observed hole mobility is typical for columnar phases formed by polycyclic aromatic derivatives[6,18] and its weak temperature dependence suggests a hopping mechanism for charge transport. Also the same order of magnitude for charge mobility observed in all three materials, **1[0]**, **1[12]** and the mixture **1[0]**–**1[12]**, indicates that there are no fundamental differences in the bulk structure and no additional deep level traps in electronic conduction.

Further measurements of **1[0]**, **1[12]** and the **1[0]**–**1[12]** mixture in the same electro-optical cells demonstrated dark conductivity in the unaligned *Col*$_h$ mesophase on the order of 10^{-11} S cm^{-1} for **1[0]** and the mixture, while for **1[12]** an order of magnitude smaller (Figure 15 bottom). The current increased 2–4 times during irradiation of the samples with UV light. For instance, at 50 °C the dark current was 4.8, 0.9 and 8.1×10^{-11} S cm^{-1} for **1[0]**, **1[12]** and the **1[0]**–**1[12]** mixture, respectively, while during illumination with a 365 nm UV-LED lamp it increased to 7.8, 3.5 and 13.3×10^{-11} S cm^{-1}, respectively at 1 Hz.

Magnetization studies revealed ferromagnetic interactions in the fresh solid sample similar to those found in pure **1[12]** (Figure 16), but with a smaller ferromagnetic exchange interaction ($J/k_B = 1.96(3)$ K *vs* 7.48(4) K). On the other hand, the binary mixture cooled from the isotropic phase shows magnetic behavior similar to lower members of series **1[n]**, in which only antiferromagnetic interactions are observed at lower temperatures. This is presumably due to large degree of glassification of the *Col*$_h$ phase, as evident from a small decrease in $\chi_p\cdot T$ values at 287 K.

3. Summary and Conclusions

Series **1[n]** represents a rare, self-organizing, multi-phase system, in which magnetic properties are substituent-dependent in all three phases: isotropic liquid, columnar and crystalline with abrupt changes between them. Magnetization at the *Col*$_h$–Cr transition decreases for low homologues

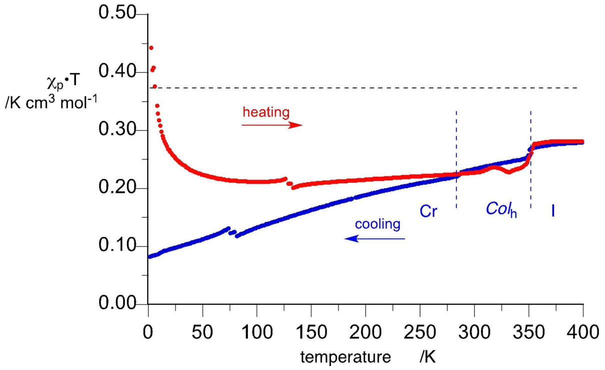

Figure 16. $\chi_p \cdot T$ *vs* temperature plot for a 1:1 mixture of **1[0]** and **1[12]** obtained on first heating (red) and subsequent cooling (blue). Temperature change rate 0.8 K min^{-1}, field 0.1 T. The horizontal line marks the 0.375 K cm^3 mol^{-1} value. Vertical dashed lines mark phase transitions. The diamagnetic correction obtained on heating was used for analysis of both curves. The discontinuity at about 75 and 125 K is due to magnetization crossing zero.

(antiferromagnetic interactions in half discs) and increases in high homologues (ferromagnetic interactions in full discs).

Results suggest that nanosegregation of the molecules and column formation drive the co-facial alignment of the spin-containing cores, while the size of the N(1)–Ar substituent affects the intermolecular contact and the strength of antiferromagnetic interactions. As evident from powder XRD studies, the increasing size of the N(1)–Ar substituent and consequently change of the molecular shape causes a gradual modification of molecular packing in the columns. This, in turn, results in increasing concentration of uncompensated spins in all three phases and increasing strength of ferromagnetic interactions in the crystalline phase. The strength of these interactions also depends on thermal history of the sample. The strongest ferromagnetic exchange interactions were found in the fully crystalline sample of **1[12]** ($J/k_B = 7.48(5)$ K), which can be ascribed to local interactions of average 5–6 spins in a 1D chain.

Electric measurements revealed hole mobility and dark electric conduction typical for unaligned discotic materials (~ 10^{-3} cm^{2}V^{-1}s^{-1} and ~10^{-11} S cm^{-1}, respectively). The latter increases upon illumination with UV light due to generated additional charge carriers. Data indicates that increasing size of the N(1)–Ar substituent results in slight decrease in hole mobility and conductivity with simultaneous increase of ferromagnetic interactions in the homologous series due to the expanded distance between the cores.

Formation of mixtures expands the range of the columnar mesophase without significantly affecting the charge transport properties, but it modulates magnetic behavior of the materials. This opens a possibility for controlling material's properties by structure, composition, and thermal history in the context of transporting spin information.

Experimental Section

General. Reagents and solvents were purchased (Sigma-Aldrich, Acros) and used as received without further purification. Tetrahydrofuran was dried over sodium metal in the presence of benzophenone and distilled just before usage. Products were purified by flash chromatography on silica gel (230–400 mesh, Merck or Fluka). Reported yields refer to analytically pure samples. NMR spectra of non-radical intermediates were measured with a Bruker AVIII 600 instrument. Chemical shifts are reported relative to solvent peaks (^{1}H NMR: $\delta = 7.26$ ppm [CDCl$_3$]; $\delta = 2.50$ ppm [DMSO-d_6]; ^{13}C NMR: $\delta = 77.0$ ppm [CDCl$_3$]). For peak assignment in ^{13}C NMR 2D spectra were obtained (COSY, HMQC, HMBC). IR spectra were measured with a FTIR spectrometer as KBr pellets or thin films. ESI-MS spectra were performed with a Varian 500-MS LC Ion Trap. Positive ion MALDI mass spectra were recorded on the Voyager-Elite instrument in reflector mode. A 10 mg/mL solution of α-cyano-4-hydroxycinnaminic acid (CHA) in THF was used as the matrix. The synthesis of radicals **1[n]** was carried out under argon in a flame-dried flask with addition of the reactants by a syringe; subsequent manipulations were conducted in air.

Preparation of 1,4-Dihydrobenzo[*e*][1,2,4]triazin-4-yl Radicals 1[n]: A General Procedure: An excess solution of appropriate aryllithium (*ca.* 0.40-0.50 mmol) in dry THF was added dropwise at 0 °C to a magnetically stirred solution of benzo[*e*][1,2,4]triazine **2** (278 mg, 0.2 mmol) in dry THF (2.5 mL) under Ar atmosphere. The mixture was kept at rt for 30 min, then it was opened to air, then diluted with dry petroleum ether (*ca.* 20 mL), and the stirring was continued for 1.5 h. Resulting mixture was filtered through short plug of Celite, the solvents were removed under reduced pressure, and the crude product was washed with hot MeCN (3×60 mL) to remove byproducts, mainly the 3,4,5-trialkoxybenzene. Purification by column chromatography on silica gel (SiO$_2$ deactivated with 2% Et$_3$N in petroleum ether before use; petroleum ether/Et$_2$O 5:1; visualization with the *p*-anisaldehyde stain) provided **1[n]**, which was recrystallized 4–6 times from a MeCN/EtOAc mixture.

Preparation of Aryllithium Reagents: A General Procedure: To a solution of the corresponding 1-bromo-3,4,5-trialkoxybenzene (**3[n]**, 0.6 mmol, for details see the SI) in dry THF (10 mL), a solution of *tert*-BuLi (1.7 M in pentane, 0.78 mL, 1.32 mmol) was added dropwise at −40 °C (due to limited solubility of bromides **3[10]** and **3[12]** in THF at low temperatures, the addition of *tert*-BuLi was performed at −25 °C). The resulting mixture was stirred at this temperature until the starting bromide was fully consumed (typically *ca.* 20–30 min, TLC monitoring of samples quenched with acetone; SiO$_2$, petroleum ether/dichloromethane 3:1, visualization with *p*-anisaldehyde stain), and the cooling bath was removed to allow the mixture to slowly warm up. After the yellow color of the solution faded indicating decomposition of excess *tert*-BuLi, the mixture was cooled to −40 °C, and immediately used for subsequent step.

1-Phenyl-3,6-bis(3,4,5-tridodecyloxyphenyl)-1,4-dihydrobenzo[*e*][1,2,4]triazin-4-yl (1[0]):[7] Commercially available PhLi (1.9 M solution in Bu$_2$O) was used for the reaction with benzo[*e*][1,2,4]triazine **2**; olive solid, yield 214 mg (73%).

3,6-Bis(3,4,5-tridodecyloxyphenyl)-1-(3,4,5-trimethoxyphenyl)-1,4-dihydrobenzo[*e*][1,2,4]triazin-4-yl (1[1]): Brown solid, yield 283 mg (91%); IR (KBr) *ν* 2920, 2851, 1594, 1501, 1468, 1231, 1126 cm^{-1}; MALDI-MS (*m/z*) 1556.6 (100, [M]$^+$). Anal. Calcd for $C_{100}H_{168}N_3O_9$: C, 77.17; H, 10.88; N, 2.70. Found: C, 77.14; H, 10.85; N, 2.68.

3,6-Bis(3,4,5-tridodecyloxyphenyl)-1-(3,4,5-triethoxyphenyl)-1,4-dihydrobenzo[*e*][1,2,4]triazin-4-yl (1[2]): Brown solid, yield 284 mg (89%); IR (KBr) *ν* 2921, 2851, 1588, 1469, 1387, 1120 cm^{-1}; MALDI-

MS (m/z) 1598.6 (100, [M]$^+$). Anal. Calcd for $C_{103}H_{174}N_3O_9$: C, 77.39; H, 10.97; N, 2.63. Found: C, 77.23; H, 10.85; N, 2.42.

1-(3,4,5-Tributoxyphenyl)-3,6-bis(3,4,5-tridodecyloxyphenyl)-1,4-dihydrobenzo[*e*][1,2,4]triazin-4-yl (1[4]): Brown solid, yield: 239 mg (71 %); IR (KBr) ν 2920, 2851, 1592, 1468, 1432, 1231, 1115 cm^{-1}; MALDI-MS (m/z) 1682.5 (100, [M]$^+$). Anal. Calcd for $C_{109}H_{186}N_3O_9$: C, 77.80; H, 11.14; N, 2.50. Found: C, 77.89; H, 11.04; N, 2.46.

3,6-Bis(3,4,5-tridodecyloxyphenyl)-1-(3,4,5-trihexyloxyphenyl)-1,4-dihydrobenzo[*e*][1,2,4]triazin-4-yl (1[6]): Brown-green solid; yield 279 mg (79 %); IR (KBr) ν 2922, 2851, 1590, 1468, 1114 cm^{-1}; MALDI-MS (m/z) 1766.7 (100, [M]$^+$). Anal. Calcd for $C_{115}H_{198}N_3O_9$: C, 78.18; H, 11.30; N, 2.38. Found: C, 78.21; H, 11.32; N, 2.24.

3,6-Bis(3,4,5-tridodecyloxyphenyl)-1-(3,4,5-trioctyloxyphenyl)-1,4-dihydrobenzo[*e*][1,2,4]triazin-4-yl (1[8]): Olive solid; yield 252 mg (68 %); IR (KBr) ν 2923, 2852, 1591, 1468, 1226, 1115 cm^{-1}; MALDI-MS (m/z) 1850.4 (100, [M]$^+$). Anal. Calcd for $C_{121}H_{210}N_3O_9$: C, 78.52; H, 11.44; N, 2.27. Found: C, 78.77; H, 11.39; N, 2.21.

1-(3,4,5-Tridecyloxyphenyl)-3,6-bis(3,4,5-tridodecyloxyphenyl)-1,4-dihydrobenzo[*e*][1,2,4]triazin-4-yl (1[10]): Olive solid; yield 321 mg (83 %); IR (KBr) ν 2956, 2920, 2851, 1589, 1468, 1408, 1115 cm^{-1}; MALDI-MS (m/z) 1934.9 (100, [M]$^+$). Anal. Calcd for $C_{127}H_{222}N_3O_9$: C, 78.82; H, 11.56; N, 2.17. Found: C, 78.78; H, 11.60; N, 2.09.

1,3,6-Tris(3,4,5-tridodecyloxyphenyl)-1,4-dihydrobenzo[*e*][1,2,4]triazin-4-yl (1[12]).[7] Yield: 321 mg (80 %).

Preparation of 1-Bromo-3,4,5-trialkoxybenzene (3[n]): A General Procedure: A mixture of freshly prepared 1-bromo-3,4,5-trihydroxybenzene[10] (1.02 g, 5.0 mmol) and K_2CO_3 (4.15 g, 30.0 mmol) in dry DMF (40 mL) was stirred at room temperature for 30 min. Then, appropriate alkyl bromide (20.0 mmol) was added, and the mixture was heated under inert atmosphere overnight at 75 °C. After cooling, the resulting mixture was diluted with water (150 mL) and organic products extracted with hexanes (3×30 mL). Combined organic layers were dried (Na_2SO_4), solvents were removed in *vacuo*, and the residue was purified by column chromatography (SiO_2, pet. ether/CH_2Cl_2 3:1). The products were dried under vacuum to afford pure **3[n]** in about 90 % yield as colourless low melting solids or oils (**3[6]** and **3[8]**). Full analytical data is provided in the SI.

Preparation of Binary Mixtures: A mixture of known amounts of radicals **1[0]** (0.5–1.5 mmol) and **1[12]** (0.5–1.5 mmol) was placed in a small vial and 1,2-dichloroethane (0.1 mL) was added. The mixture was heated and stirred with a spatula at 50 °C to give a homogenous solution. Then, the solvent was removed under stirring at about 80 °C, the resulting mixture was vacuum dried and analysed by POM to confirm homogeneity. Each mixture was analysed by DSC in 3 heating/cooling cycles at a rate of 5 K min^{-1}.

Powder XRD Measurements: X-ray diffraction experiments in broad angle range were performed using a Bruker D8 GADDS system (parallel Cu Kα beam formed by Göbel mirror and 0.5 mm point collimator, area detector Vantec 2000) equipped with a modified Linkam heating stage. For precise determination of lattice parameters, temperature evolution a Bruker D8 Discover system was used (parallel Cu Kα radiation, Göbel mirror monochromator, Anton Paar DCS350 heating stage, scintillation counter). Samples were prepared in a form of droplet or thin film on flat heated surface.

Magnetization Measurements: Magnetic susceptibility measurements for **1[n]** were conducted using a SQUID magnetometer (Quantum Design MPMS-XL-7T) in heating (2 K →400 K) and cooling (400 K→2 K) cycles at a rate 0.8 K min^{-1} in a magnetic field of 0.1 T. Details and data analysis are provided in the SI.

Charge Mobility and Dark Conductivity Measurements: Electric measurements of a binary mixture of **1[0]**–**1[12]** were conducted in a thin electro-optical cell. Charge mobility was obtained using the TOF (time-of-flight) method and a nitrogen gas laser at $\lambda = 337$ nm. The conductivity for **1[0]**, **1[12]** and a 1:1 binary mixture **1[0]**–**1[12]** was measured by the parallel plate capacitor method using a LCR meter in a frequency range of 0.1 Hz to 1 MHz at 0.1 V. Details and data analysis are provided in the SI.

Supplementary information

It contains further information on full details of synthesis and characterization of series **3[n]**, NMR spectra, additional DSC, XRD, magnetization, and conductivity details.

Acknowledgements

Financial support was provided by the FNP (TEAM-3/2016-3/24), National Science Center of Poland (2013/09/B/ST5/01230, 2013/11/B/ST3/04193, 2014/13/B/ST5/04525) grants.

Conflict of Interest

The authors declare no conflict of interest.

Keywords: columnar phase · liquid crystals · magnetic properties · stable radicals · synthesis

[1] a) *Organic Spintronics* Z. V. Vardeny, Ed.; CRC Press, **2017**; b) M. P. de Jong, *Open* **2016**, *14*, 337–353; c) *Organic Electronics: Emerging Concepts and Technologies*, F. Cicoira and C. Santato, Eds; Wiley-VCH, **2013**; d) D. Sun, E. Ehrenfreund, Z. V. Vardeny, *Chem. Commun.* **2014**, *50*, 1781–1793.

[2] a) C. Herrmann, G. C. Solomon, M. A. Ratner, *J. Am. Chem. Soc.* **2010**, *132*, 3682–3684; b) C. Herrmann, G. C. Solomon, M. A. Ratner, *J. Chem. Phys.* **2011**, *134*, 224306; c) M. Smeu, G. A. DiLabio, *J. Phys. Chem. C* **2010**, *114*, 17874–17879; d) K. V. Raman, A. M. Kamerbeek, A. Mukherjee, N. Atodiresei, T. K. Sen, P. Lazić, V. Caciuc, R. Michel, D. Stalke, S. K. Mandal, S. Blügel, M. Münzenberg, J. S. Moodera, *Nature*, **2013**, *493*, 509–513.

[3] a) G. Szulczewski, S. Sanvito, M. Coey, *Nat. Mater.* **2009**, *8*, 693–695; b) K. Ando, S. Watanabe, S. Mooser, E. Saitoh, H. Sirringhaus, *Nat. Mater.* **2013**, *12*, 622–627.

[4] a) P. Hui, R. Chandrasekar, *ChemPlusChem* **2012**, *77*, 1062–1065; b) P. Hui, R. Chandrasekar, *Adv. Mater.* **2013**, *25*, 2963–2967.

[5] P. Ravat, T. Marszalek, W. Pisula, K. Müllen, M. Baumgarten, *J. Am. Chem. Soc.* **2014**, *136*, 12860–12863.

[6] W. Pisula, K. Müllen, in *Hanbook of Liquid Crystals, Vol. 8* (Eds.: J. W. Goodby, P. J. Collings, T. Kato, C. Tschierske, H. F. Gleeson, P. Raynes), Wiley-VCH, Mörlenbach, Germany, **2014**, pp. 627–673.

[7] M. Jasiński, J. Szczytko, D. Pociecha, H. Monobe, P. Kaszyński, *J. Am. Chem. Soc.* **2016**, *138*, 9421–9424.

[8] a) C. P. Constantinides, P. A. Koutentis, *Adv. Heterocycl. Chem.* **2016**, *119*, 173–207; b) C. P. Constantinides, P. A. Koutentis, H. Krassos, J. M. Rawson, A. J. Tasiopoulos, *J. Org. Chem.* **2011**, *76*, 2798–2806; c) *Stable radicals: fundamentals and applied aspects of odd-electron compounds*, R. G. Hicks, Ed.; Wiley & Sons, Chichester, **2010**.

[9] C. P. Constantinides, E. Obijalska, P. Kaszyński, *Org. Lett.* **2016**, *18*, 916–919.

[10] For details see the Supporting Information.

[11] T. Yasuda, T. Shimizu, F. Liu, G. Ungar, T. Kato, *J. Am. Chem. Soc.* **2011**, *133*, 13437–13444.

[12] G. A. Baker, Jr., G. S. Rushbrooke, H. E. Gilbert, *Phys. Rev.* **1964**, *135*, A1272–A1277.

[13] a) A. Jankowiak, D. Pociecha, H. Monobe, J. Szczytko, P. Kaszyński, *Chem. Commun.* **2012**, *48*, 7064–7066; b) A. Jankowiak, D. Pociecha, J. Szczytko, H. Monobe, P. Kaszyński, *J. Am. Chem. Soc.* **2012**, *134*, 2465–2468; c) A. Jankowiak, D. Pociecha, J. Szczytko, P. Kaszyński, *Liq. Cryst.* **2014**, *41*, 1653–1660.

[14] S. Castellanos, F. López-Calahorra, E. Brillas, L. Juliá, D. Velasco, *Angew. Chem. Int. Ed.* **2009**, *48*, 6516–6519; *Angew. Chem.* **2009**, *121*, 6638–6641.

[15] R. Tamura, Y. Uchida, K. Suzuki, in *Handbook of Liquid Crystals, Vol. 8* (Eds.: J. W. Goodby, P. J. Collings, T. Kato, C. Tschierske, H. F. Gleeson, P. Raynes), Wiley-VCH, Weinheim, **2014**, pp. 837–864.

[16] S. Kapuściński, A. Gardias, D. Pociecha, M. Jasiński, J. Szczytko, P. Kaszyński, *J. Mater. Chem. C* **2018**, *6*, 3079–3088.

[17] H. M. McConnell, *J. Chem. Phys.* **1963**, *39*, 1910.

[18] a) B. R. Kaafarani, *Chem. Mater.* **2011**, *23*, 378–396; b) R. J. Bushby, D. J. Tate, in *Liquid Crystalline Semiconductors* (Eds.: R. J. Bushby, S. M. Kelly), Springer Science, Dordrecht, **2013**, pp. 65–96.

Manuscript received: October 16, 2018
Revised manuscript received: December 19, 2018
Version of record online: ■■, ■

ARTICLES

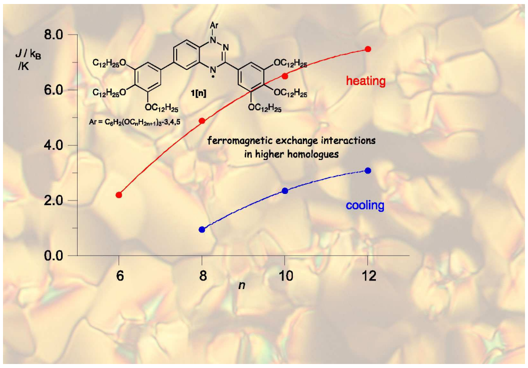

Dr. M. Jasiński, K. Szymańska, A. Gardias, Dr. D. Pociecha, Dr. H. Monobe, Dr. J. Szczytko, Prof. P. Kaszyński

1 – 10

Tuning the Magnetic Properties of Columnar Benzo[*e*][1,2,4]triazin-4-yls with the Molecular Shape

The magnitude of the ferromagnetic exchange interaction *J* in series **1[n]** is tuned by the size of the Ar substituent at the N(1) position (shape of the molecular disc) and by the formation of binary mixtures.